Nano Research 2016, 9(5): 1418–1425
DOI 10.1007/s12274-016-1037-6
Research Article
ISSN 1998-0124
CN 11-5974/O4

Stable and unique graphitic Raman internal standard nanocapsules for surface-enhanced Raman spectroscopy quantitative analysis

Yuxiu Zou[1,§], Long Chen[2,§], Zhiling Song[1], Ding Ding[1], Yiqin Chen[3], Yiting Xu[1], Shanshan Wang[1], Xiaofang Lai[1], Yin Zhang[1], Yang Sun[1], Zhuo Chen[1] (✉), and Weihong Tan[1] (✉)

[1] *Molecular Science and Biomedicine Laboratory, State Key Laboratory of Chemo/Bio-Sensing and Chemometrics, College of Chemistry and Chemical Engineering, College of Biology, Hunan University, Changsha 410082, China*
[2] *Faculty of Science and Technology, University of Macau, E11, Avenida da Universidade, Taipa, Macau 999078, China*
[3] *School of Physics and Electronics, State Key Laboratory for Chemo/ Biosensing and Chemometrics, Hunan University, Changsha 410082, China*
[§] *These authors contributed equally to this work.*

Received: 25 December 2015
Revised: 29 January 2016
Accepted: 3 February 2016

KEYWORDS

graphitic nanomaterials, analytical methods, internal standards, quantitative analysis, surface-enhanced Raman spectroscopy (SERS)

ABSTRACT

Graphitic nanomaterials have unique, strong, and stable Raman vibrations that have been widely applied in chemistry and biomedicine. However, utilizing them as internal standards (ISs) to improve the accuracy of surface-enhanced Raman spectroscopy (SERS) analysis has not been attempted. Herein, we report the design of a unique IS nanostructure consisting of a large number of gold nanoparticles (AuNPs) decorated on multilayered graphitic magnetic nanocapsules (AGNs) to quantify the analyte and eliminate the problems associated with traditional ISs. The AGNs demonstrated a unique Raman band from the graphitic component, which was localized in the Raman silent region of the biomolecules, making them an ideal IS for quantitative Raman analysis without any background interference. The IS signal from the AGNs also indicated superior stability, even under harsh conditions. With the enhancement of the decorated AuNPs, the AGN nanostructures greatly improved the quantitative accuracy of SERS, in particular the exclusion of quantitative errors resulting from collection loss and non-uniform distribution of the analytes. The AGNs were further utilized for cell staining and Raman imaging, and they showed great promise for applications in biomedicine.

1 Introduction

Surface-enhanced Raman spectroscopy (SERS) is a widely used analytical method capable of providing valuable information about the chemical structure and composition of molecules [1–6]. However, relatively

Address correspondence to Zhuo Chen, zhuochen@hnu.edu.cn; Weihong Tan, tan@chem.ufl.edu

few quantitative SERS applications have been developed because optical methods must contend with intensity variations produced by changes in excitation, collection efficiency, or both. Adding an internal standard (IS) to analyze the intensity variations has been proposed for employing SERS technology in quantitative analysis, and its implementation has proven to be highly reliable [7–9]. The introduction of an IS can eliminate the influence of surface heterogeneity in the enhancing substrate, which is known to cause significant variations in absolute SERS intensities. However, conventional IS methods have encountered unstable IS SERS signals, interference from the analyte or impure molecules, and insufficient SERS enhancement.

Graphitic nanomaterials possess unique optical properties, especially distinctive Raman signatures. High-scattering cross sections, as well as resonance and surface enhancement, make them ideal for sensitive Raman detection and imaging [10–13]. However, utilizing graphitic nanomaterials as ISs to improve the accuracy of SERS analysis has never been attempted. As compared to traditional IS molecules, graphitic nanomaterials offer benefits because of their simple and unique spectra, resulting in less background interference. By their stable and robust signals, graphitic nanomaterials are not subject to photobleaching or photoquenching, characteristics that make them ideal candidates as IS molecules. Therefore, we designed a unique IS nanostructure consisting of a large number of gold nanoparticles decorated on multilayered graphitic magnetic nanocapsules, termed AGNs, achieving very high and stable Raman enhancement effects. The graphitic shell expressed a strong Raman vibration band in the Raman silent region (1,800–2,800 cm^{-1}) [14], which could be ideally used as an IS for SERS quantitative analysis based on less interference from the vibration peaks of environmental biomolecules. Such a strategy integrates high enhancement and stability into single bionanoparticles, thereby affording an AGN IS with dual advantages of improved quantitative accuracy and high sensitivity.

2 Results and discussion

2.1 Synthesis and characterization of AGNs

AGNs were fabricated as multilayered core–shell structures. Figure 1(a) shows a schematic diagram of the prepared AGN nanostructure, with a magnetic core and a multilayered graphene shell decorated with gold nanoparticles. Magnetic–multilayer graphitic nanocapsules (MMs) were negatively charged after treating them with a sulfuric and nitric acid solution to acquire water solubility (Fig. 1(b), $\zeta = -25$ mV). Positively charged

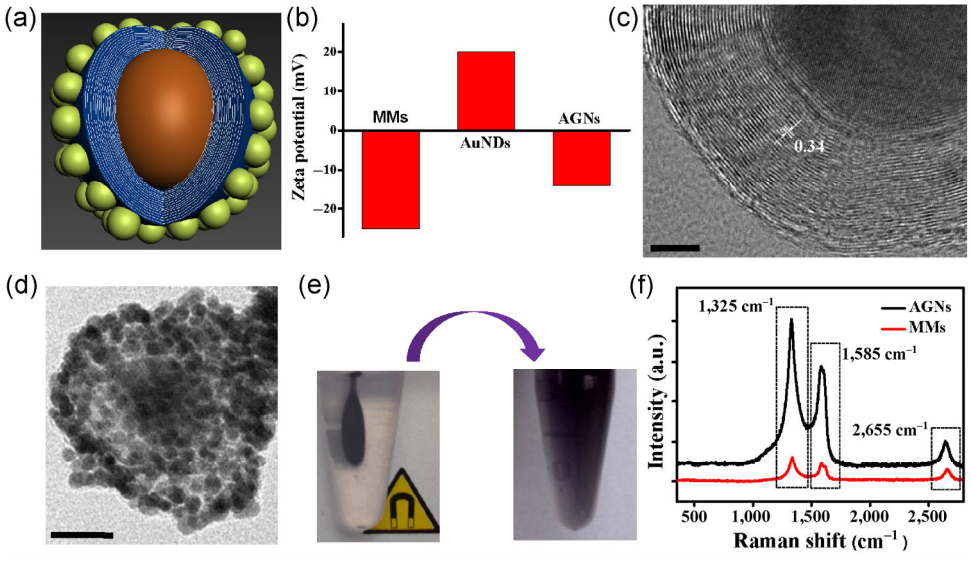

Figure 1 AGN synthesis and characterization. (a) Schematic diagram of AGNs. (b) Zeta potentials of MMs, gold seeds, and AGNs. (c) HR-TEM image of MMs, with arrows showing the 0.34 nm lattice constant of the graphitic layer; scale bar: 5 nm. (d) TEM image of single AGN; scale bar: 20 nm. (e) Digital photos of AGN solution under external magnet (left) and then redispersed with water (right). (f) Raman spectra of MMs (red) and AGNs (black).

gold seeds (Fig. 1(b), ζ = +20 mV) were decorated on the surfaces of the MMs (Fig. S1(a) in the Electronic Supplementary Material (ESM)) through electrostatic interactions. As shown in Fig. 1(b), after the growth of the gold seeds, the ζ potential of the final AGNs increased to −14 mV, a remarkable increase from that of MMs as a result of AuNP adhesion. Transmission electron microscopy (TEM) and high-resolution TEM (HR-TEM) were utilized to characterize the MM and AGN nanocapsules. As exhibited in Fig. 1(c) and Fig. S1(b) (in the ESM), the magnetic core was encapsulated in the multilayer shell. The space between shell layers was ~0.34 nm, which is consistent with the interlayer distance of graphite. The AuNPs decorating the surfaces of the MM nanocapsules are shown in Fig. 1(d). The AGN nanocapsules showed significant magnetism. As demonstrated in Fig. 1(e), AGNs were separated from the aqueous solution under an external magnet and redispersed, thus facilitating sample enrichment and separation and making the process of nanocapsule fabrication simple and easy. The surfactant 4-dimethylaminopyridine (DMAP), which was inherited from the AGN synthesis, showed strong Raman vibrations (Fig. S1(c) in the ESM), but it was completely removed by magnetic separation without sacrificing the stability of the nanocapsules. In addition, the AGN nanocapsules demonstrated simple, strong, and unique Raman scattering properties. Figure 1(f) shows the Raman spectra of the MMs with and without AuNPs. Two prominent bands can be observed at approximately 1,325 and 1,585 cm^{-1}, corresponding to the D and G Raman vibrational modes, respectively, of graphitic carbon shells. A second-order 2D peak was observed at approximately 2,655 cm^{-1}, which lies in the Raman silent region. The intensively packed gold nanoparticles significantly enhanced all graphitic Raman vibrations, resulting in a significant SERS effect. The unique 2D band is strong enough for use as an ideal intrinsic IS for SERS quantitative analysis.

2.2 SERS behavior optimization

Pursuing a high surface enhancement effect is critical for Raman analysis with AGNs. Because SERS enhancement efficiency is associated with substrate roughness, the decoration of AuNPs on the surfaces of AGN nanocapsules is essential to Raman signal enhancement. By modulating the growth of gold seeds [15], AuNPs of different sizes were obtained, forming, in turn, unique assembled nanostructures. The ultraviolet/visible (UV/vis) absorption spectra of three successively grown AGN nanostructures are shown in Fig. 2(a). The plasmon resonance was progressively red-shifted and became increasingly broader as the size of the AuNPs increased. The AGN solutions with different gold nanometer architectures were also observed to change color, as shown in the insets of Figs. 2(b)–2(d). Such unique nanostructures were also characterized with TEM. Figures 2(b)–2(d) show three sizes of AuNPs of approximately 5, 7, and 12 nm, respectively. More TEM images of MMs are shown in Fig. S2 (in the ESM). From MMs to AGNs, the average hydrodynamic radius increased from 80 to 120 nm when decorated with 12 nm AuNPs (Fig. S2(b) in the ESM).

The finite difference time-domain (FDTD) method was utilized to simulate the space electric field distribution of the AGNs [16]. The geometry used for our simulations was that of a single sphere covered with a large number (158) of gold spheres (Fig. 2(e)(1)). The AuNPs had an average diameter of 12 nm (right) and 5 nm (left), indicating two different gold growth stages. Figure 2(e)(2) shows the simulation of AGN under excitation by a laser with a source frequency of 633 nm. The AuNPs were attached to the MM core in a random manner, which caused the inhomogeneous electric field distributions in the AGN. The electric field intensity sharply increased as the AuNPs grew larger, which is consistent with the Raman enhancement effect of AGNs having two different nanostructures (Fig. 2(f)). Rhodamine B (RhB) was used as a model molecule for the SERS effect comparison. The signal enhancement of AGNs with 12 nm AuNPs was approximately two times higher than that of AGNs with 5 nm AuNPs according to the 618 cm^{-1} band of RhB. Thus, nanocapsules with a higher surface plasmon resonance effect were used in the following SERS applications.

2.3 Stability and SERS quantitative accuracy of AGNs

With good surface plasmon resonance properties and unique Raman vibrations, we then investigated the use

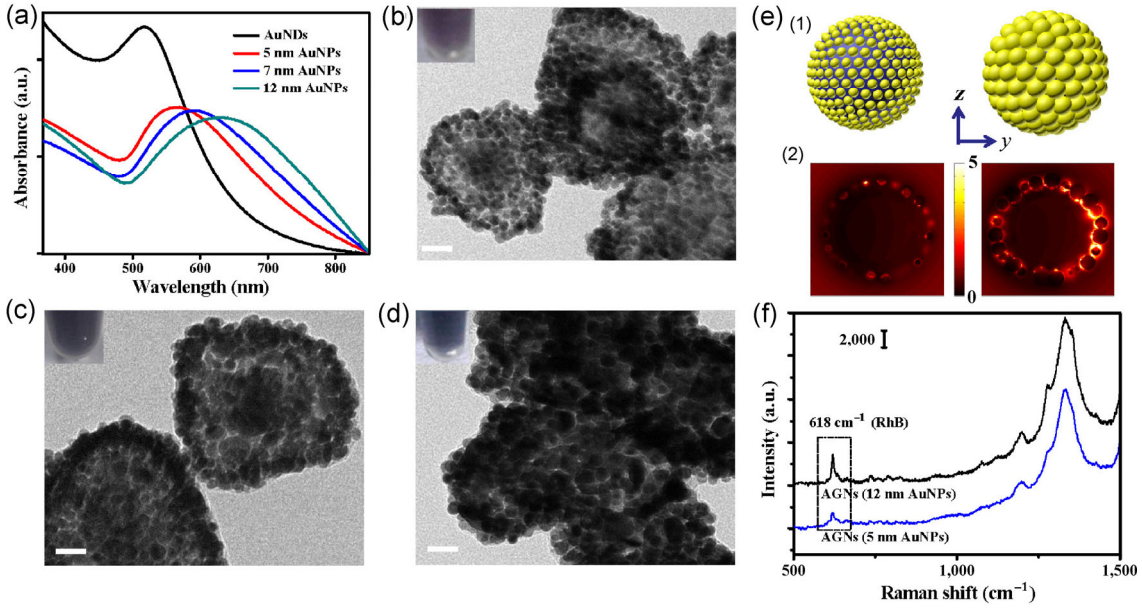

Figure 2 Modulating the growth of gold seeds on MMs. (a) UV/vis spectra of gold seeds (black), AGNs with distribution of AuNPs in three sizes. TEM images of AGNs with (b) 5 nm (red), (c) 7 nm (blue), and (d) 12 nm (green) AuNPs. Insets are respective digital photos of the AGN solutions; scale bar: 20 nm. (e)(1) FDTD simulation models with an average diameter of 12 nm (right) and 5 nm (left); (e)(2) plots showing simulated results of electric field distribution relative to (1). (f) Raman spectra of 0.2 μL RhB (10 μM) with AGNs with 12 and 5 nm AuNPs.

of AGNs as a Raman IS. For comparison, p-toluenethiol (pTSH), a conventional organic IS molecule [17], was also used. Figure 3(a) shows the Raman spectra of AuNP@pTSH, whereas Fig. 3(b) shows those of AGNs before and after adding a 15% H_2O_2 solution (Figs. 3(a) and 3(b) and Fig. S3(a) in the ESM). The SERS intensity of Au@pTSH decreased after 20 min, whereas the AGNs showed superior signal stability, indicating their suitability as IS molecules. The instability of the Au@pTSH signal could be attributed to the destruction of the Au–S bond by H_2O_2, whereas the graphitic layer of the AGNs effectively resisted such harsh environmental conditions. The AGNs also demonstrated an excellent enhancement effect as SERS substrates. The Raman signals of molecules adsorbed onto AGNs could be enhanced by several orders of magnitude. RhB molecules were used for detection and determination of the SERS effect (Fig. 3(c)). When RhB was added to the AGN SERS substrates and dried, the Raman signals were significantly enhanced more than 10^6 times.

Utilizing AGNs as the IS eliminated the influence of surface heterogeneity in the enhancing substrate and significantly improved Raman analysis accuracy. In the RhB detection model system, the IS band (2,655 cm^{-1}) of the AGNs lying in the silent region was ideal for RhB detection without any covering or overlaying of the Raman signal from RhB molecules. We then varied the focus depth of the laser beam to 5, 4, 3, 2, and 1 μm (Fig. 3(d)). Two bands at 618 cm^{-1} from RhB and 2,655 cm^{-1} from the AGN IS were indicated (Figs. 3(e) and 3(f), respectively). The peak intensity of the two Raman bands increased with decreasing distance between the laser beam and the sample surface. The band at 618 cm^{-1} of RhB and the ratio of $I_{618}/I_{2,655}$ were used for relative standard deviation (RSD, %) analysis. RSD was significantly reduced from 20.4% to 6.8% by using the AGN IS (Fig. 3(g)) to eliminate Raman signal variation arising from the measurement system. This IS strategy works better with low analyte concentrations because the Raman signal of such analytes is weak and sensitive to the mapping processes. Improved Raman detection accuracy with a corresponding reduction in RSD (%) was demonstrated with a lower RhB amount (Figs. S3(b)–S3(d) in the ESM).

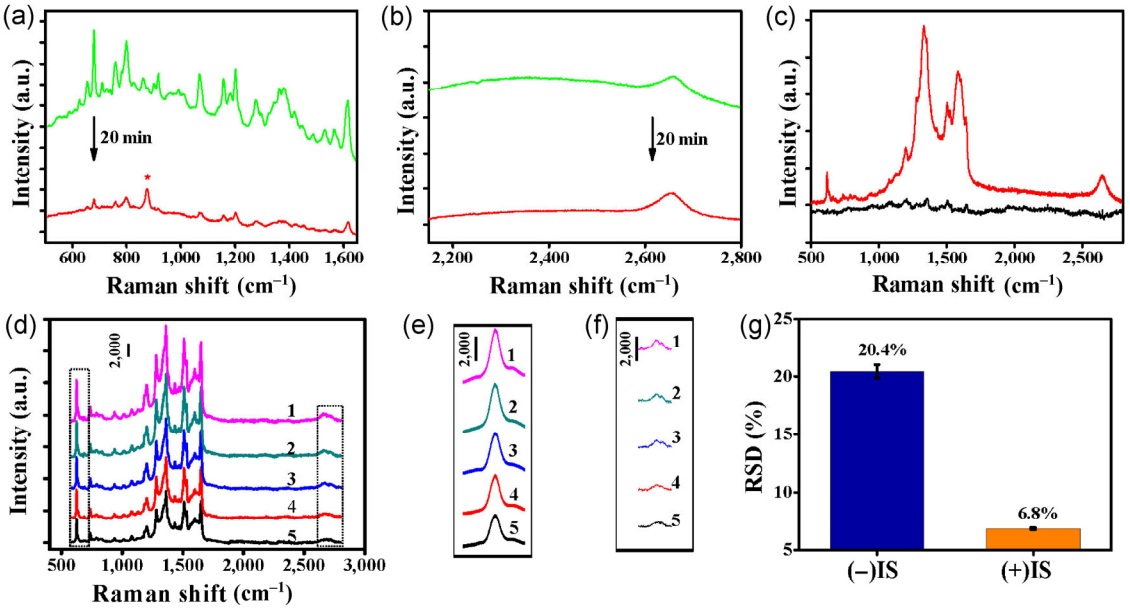

Figure 3 AGNs as a Raman IS. SERS spectra collected from (a) Au@pTSH and (b) AGNs before and after adding 15% H_2O_2 at 20 min intervals. (c) Raman spectra of 10 μM RhB with (red) and without (black) AGNs. (d) SERS spectra of RhB (30 μM) with various laser focusing depths of 5, 4, 3, 2, and 1 μm. Raman bands of (e) 618 and (f) 2,655 cm^{-1} zoom in of (d). (g) RSD (%) calculated from (d) with and without AGN internal standard normalization.

2.4 AGNs as IS for SERS Raman analysis

The AGNs were further utilized to fabricate a paper-based SERS substrate. Paper has been used as a supporting material [18, 19] because it is flexible, thin, and lightweight. It also has a perfect adsorption capability, in addition to being much cheaper than other substrates [20, 21]. Commercial paper with weak hydrophobicity was used for the AGN SERS substrate assembly. The concentrated AGNs were dropped onto the paper and dried. Solvent evaporation induced the formation of a closely packed array of AGNs on the paper. Owing to its weak hydrophobicity and adsorption properties, a flat substrate (2 mm × 2 mm) with a much weakened "coffee-ring effect"[22], a pattern left by a puddle of particle-laden liquid after evaporation, was obtained over the course of 30 min (Fig. S4(a) in the ESM). In contrast to other substrates such as glass and silicon, it is difficult to form a flat SERS substrate in a short time, again owing to the "coffee-ring effect" (Fig. S4(b) in the ESM). Moreover, the paper-based SERS substrate exhibited remarkably good storage stability (Fig. S4(c) in the ESM). A schematic illustration of the detection mode is shown in Fig. 4(a). With such an AGN substrate, the intensity of both the IS and the analyte could be enhanced.

Raman mapping was then utilized for RhB detection with the AGN-based paper substrate. Preparation of SERS substrates is very important because even very small variations in the size and shape of AuNP aggregation can result in the distribution of uneven hot spots. The stability of the AGN paper substrates maximized hot spot uniformity and improved quantification accuracy. Figure 4(b) shows Raman mapping images of RhB (618 cm^{-1}), IS (2,655 cm^{-1}), and the ratio calculated from I_{618}/I_{2655} with various amounts of RhB from 6.25 pmol to 40 fmol. Images with pixel sizes of 25 μm × 25 μm were generated after spectra preprocessing. For each Raman spectrum, the fluorescence background correction was conducted by polynomial fittings, and the thermal noise was suppressed by small-window moving-average smoothing [23].

Using the AGN Raman IS, SERS detection demonstrated better quantification accuracy by the reduction of quantitative error introduced by the surface heterogeneity of the SERS substrate, especially at lower RhB concentrations. Obvious RhB signals were observed within the SERS substrate at concentrations above 500 fmol. At lower concentrations, the RhB signal was sparse, which is consistent with the small number

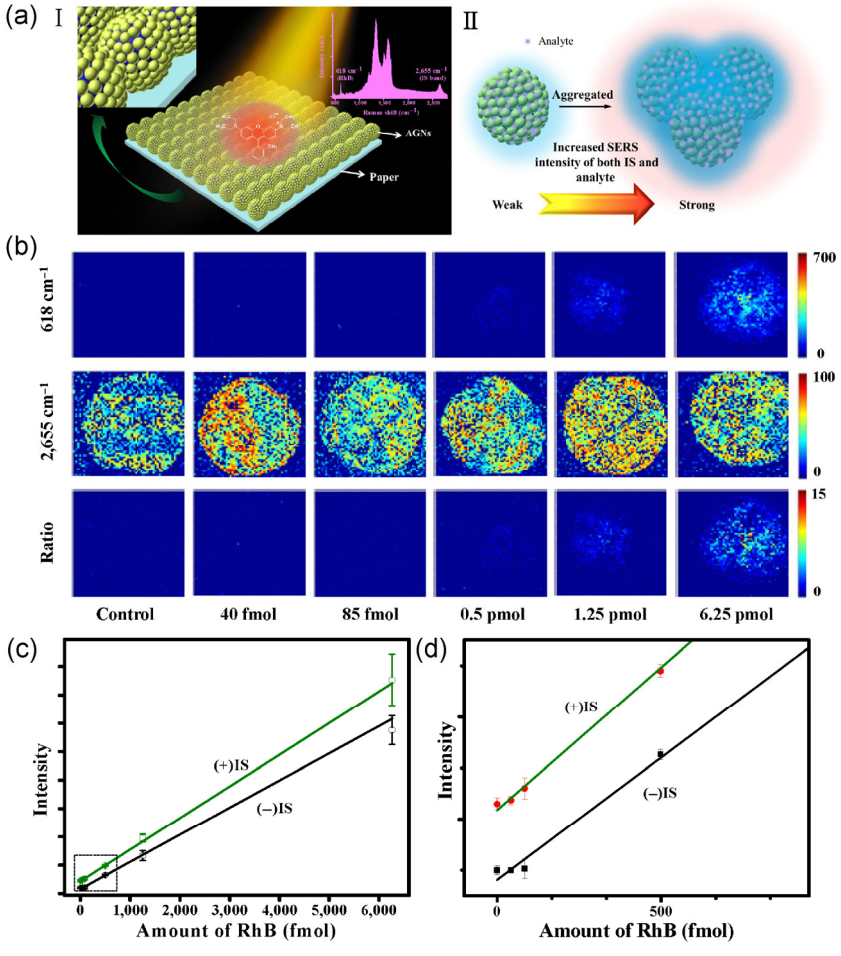

Figure 4 AGN as IS for SERS Raman analysis. (a) Schematic I: preparation of SERS substrate and Raman mapping. Bands of 618 and 2,655 cm^{-1} were used for quantitative analysis and assigned to RhB (analyte) and multilayer graphene (IS), respectively; schematic II: aggregation behavior of AGNs on the paper. (b) SERS mapping images with various amounts of RhB ranging from 40 fmol to 6.25 pmol. Each image contains approximately 3,600 pixels. First line: SERS mapping images of 618 cm^{-1}; second line: SERS mapping images of 2,655 cm^{-1}; third line: mapping images of ratio where each pixel represents a ratio value ($I_{618}/I_{2,655}$). (c) Calibration curve, (+)IS (green) and (−)IS (black), the signal of 618 cm^{-1} was normalized. (d) High magnification of region marked in (c).

of RhB molecules. The results represent the response of 3,600 points (pixels). As shown in Fig. 4(b), different aggregation states of AGNs were demonstrated in the Raman mapping images. However, using the 2,655 cm^{-1} band as the Raman IS should minimize the influence of surface heterogeneity. The bands at 618 cm^{-1} and $I_{618}/I_{2,655}$ were used for quantitative analysis (Figs. 4(c) and 4(d)) and were denoted as (–)IS and (+)IS, respectively. One-parameter linear regression was found to adequately fit the data, allowing quantification of the Raman images. It is evident from Fig. 4(c) that the curved lines of (+)IS (R^2 = 0.994) were more sensitive to concentration changes as compared to (–)IS (R^2 = 0.987), indicating that Raman analysis with an AGN IS has better detection capability at low concentrations. As shown in Fig. 4(d), when the RhB concentration was lower than 85 fmol, only (+)IS could distinguish Raman signals from those measured at control spots without any analyte. Such results could be attributed to the ability of the AGN IS to correct for possible variations that might arise from uneven hot spot distribution, changes to the laser focus depth during the large-area Raman mapping, or both.

2.5 Raman mapping images of live cells

With the strong and unique D, G, and 2D Raman bands, AGN nanocapsules were further applied for

cell staining and SERS imaging. Especially, the 2D vibration band at approximately 2,655 cm^{-1}, which lies in the Raman silent region of the cell, could be an ideal Raman tag for low-background imaging. Figure 5 shows Raman images of human breast cancer cells (MCF-7) stained without and with AGNs. Strong Raman signals were observed in the AGN-stained cells (Fig. S5 in the ESM). With low-background Raman imaging at the 2D band, as well as at the D and G bands, the AGNs were accurately located in the MCF-7 cells. The AGNs also demonstrated superior stability under enzyme and saline solutions (Fig. S6 in the ESM). Such unique cell staining and imaging capability indicates the potential for extending this IS strategy to live cell research and quantification.

3 Conclusion

We fabricated unique core–shell AGN nanocapsules and utilized them for Raman detection and analysis. By adjusting gold nanoparticle assembly on the MM surface, AGNs with a high SERS enhancement effect were obtained. The AGN nanocapsules demonstrated simple, strong, and unique D, G, and 2D Raman vibration bands from the multilayered graphitic shell. The 2D band, which lay in the Raman silent region of the cell, exhibited relatively little interference from vibration peaks of the environmental biomolecules, indicating that AGN is an ideal Raman IS. The AGN graphitic IS demonstrated superior stability and significantly improved the accuracy of the Raman analysis. The AGNs were further fabricated into a paper-based SERS substrate for Raman detection. The substrate demonstrated high analyte collection efficiency, better quantification accuracy, and better capacity to distinguish analytes in low concentrations. The AGNs also demonstrated the capacity for cell imaging. The AGNs were accurately co-localized in the cells with D, G, and 2D vibration bands, showing promise for the extension of this IS strategy to live cell research.

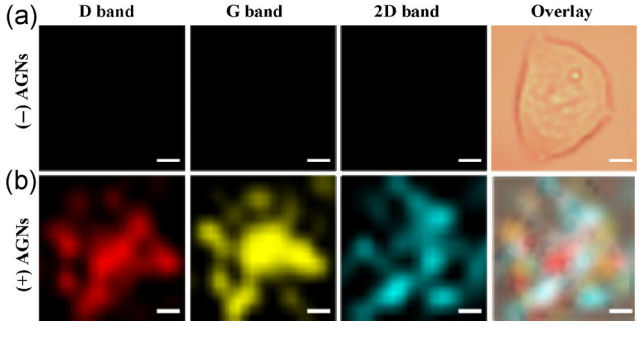

Figure 5 Raman mapping images of MCF-7 cells treated (a) without and (b) with AGNs; scale bar: 5 μm.

Acknowledgements

This work was financially supported by the National Basic Research Program of China (No. 2013CB932702), the Research Fund for the Program on National Key Scientific Instruments and Equipment Development of China (No. 2011YQ0301241402), the National Natural Science Foundation of China (No. 21522501), the Science and Technology Development Fund of Macao S.A.R (FDCT, 067/2014/A), and the Hunan Innovation and Entrepreneurship Program.

Electronic Supplementary Material: Supplementary material (experimental details, supplementary figures) is available in the online version of this article at http://dx.doi.org/10.1007/s12274-016-1037-6.

References

[1] Fu, D.; Zhou, J.; Zhu, W. S.; Manley, P. W.; Wang, Y. K.; Hood, T.; Wylie, A.; Xie, X. S. Imaging the intracellular distribution of tyrosine kinase inhibitors in living cells with quantitative hyperspectral stimulated Raman scattering. *Nat. Chem.* **2014**, *6*, 614–622.

[2] Okada, M.; Smith, N. I.; Palonpon, A. F.; Endo, H.; Kawata, S.; Sodeoka, M.; Fujita, K. Label-free Raman observation of cytochrome c dynamics during apoptosis. *Proc. Natl. Acad. Sci. USA* **2012**, *109*, 28–32.

[3] Qian, X. M.; Peng, X. H.; Ansari, D. O.; Yin-Goen, Q.; Chen, G. Z.; Shin, D. M.; Yang, L.; Young, A. N.; Wang, M. D.; Nie, S. M. *In vivo* tumor targeting and spectroscopic detection with surface-enhanced Raman nanoparticle tags. *Nat. Biotechnol.* **2008**, *26*, 83–90.

[4] Abramczyk, H.; Brozek-Pluska, B. Raman imaging in biochemical and biomedical applications. Diagnosis and treatment of breast cancer. *Chem. Rev.* **2013**, *113*, 5766–5781.

[5] Kneipp, K.; Kneipp, H.; Kneipp, J. Surface-enhanced Raman scattering in local optical fields of silver and gold nanoaggregatesfrom single-molecule Raman spectroscopy

to ultrasensitive probing in live cells. *Acc. Chem. Res.* **2006**, *39*, 443–450.

[6] Li, J. F.; Huang, Y. F.; Ding, Y.; Yang, Z. L.; Li, S. B.; Zhou, X. S.; Fan, F. R.; Zhang, W.; Zhou, Z. Y.; Wu, D. Y. et al. Shell-isolated nanoparticle-enhanced Raman spectroscopy. *Nature* **2010**, *464*, 392–395.

[7] Bell, S. E. J.; Mackle, J. N.; Sirimuthu, N. M. S. Quantitative surface-enhanced Raman spectroscopy of dipicolinic acid-towards rapid anthrax endospore detection. *Analyst* **2005**, *130*, 545–549.

[8] Deb, S. K.; Davis, B.; Knudsen, G. M.; Gudihal, R.; Ben-Amotz, D.; Davisson, V. J. Detection and relative quantification of proteins by surface enhanced Raman using isotopic labels. *J. Am. Chem. Soc.* **2008**, *130*, 9624–9625.

[9] Shen, W.; Lin, X.; Jiang, C. Y.; Li, C. Y.; Lin, H. X.; Huang, J. T.; Wang, S.; Liu, G. K.; Yan, X. M.; Zhong, Q. L. et al. Reliable quantitative SERS analysis facilitated by core–shell nanoparticles with embedded internal standards. *Angew. Chem., Int. Ed.* **2015**, *54*, 7308–7312.

[10] Chen, Z.; Tabakman, S. M.; Goodwin, A. P.; Kattah, M. G.; Daranciang, D.; Wang, X. R.; Zhang, G. Y.; Li, X. L.; Liu, Z.; Utz, P. J. et al. Protein microarrays with carbon nanotubes as multicolor Raman labels. *Nat. Biotechnol.* **2008**, *26*, 1285–1292.

[11] Liu, Z.; Tabakman, S.; Sherlock, S.; Li, X. L.; Chen, Z.; Jiang, K. L.; Fan, S. S.; Dai, H. J. Multiplexed five-color molecular imaging of cancer cells and tumor tissues with carbon nanotube Raman tags in the near-infrared. *Nano Res.* **2010**, *3*, 222–233.

[12] Xu, W. G.; Ling, X.; Xiao, J. Q.; Dresselhaus, M. S.; Kong, J.; Xu, H. X.; Liu, Z. F.; Zhang, J. Surface enhanced Raman spectroscopy on a flat graphene surface. *Proc. Natl. Acad. Sci. USA* **2012**, *109*, 9281–9286.

[13] Zheng, J.; Bai, J. H.; Zhou, Q. F.; Li, J. S.; Li, Y. H.; Yang, J. F.; Yang, R. H. DNA-templated *in situ* growth of AgNPs on SWNTs: A new approach for highly sensitive SERS assay of microRNA. *Chem. Commun.* **2015**, *51*, 6552–6555.

[14] Lin, L.; Tian, X. D.; Hong, S. L.; Dai, P.; You, Q. C.; Wang, R. Y.; Feng, L. S.; Xie, C.; Tian, Z. Q.; Chen, X. Innentitelbild: A bioorthogonal Raman reporter strategy for SERS detection of glycans on live cells. *Angew. Chem.* **2013**, *125*, 7184.

[15] Zheng, Y. Q.; Zhong, X. L.; Li, Z. Y.; Xia, Y. N. Successive, seed-mediated growth for the synthesis of single-crystal gold nanospheres with uniform diameters controlled in the range of 5–150 nm. *Part. Part. Syst. Char.* **2014**, *31*, 266–273.

[16] *Software for simulation: FDTD Solutions 8.0*; Lumerical Solutions, Inc., 2015.

[17] Chen, Y.; Chen, Z.-P.; Jin, J.-W.; Yu, R.-Q. Quantitative determination of ametryn in river water using surface-enhanced Raman spectroscopy coupled with an advanced chemometric model. *Chemom. Intell. Lab. Syst.* **2015**, *142*, 166–171.

[18] Cabalín, L. M.; Laserna, J. J. Fast spatially resolved surface-enhanced Raman spectrometry on a silver coated filter paper using charge-coupled device detection. *Anal. Chim. Acta* **1995**, *310*, 337–345.

[19] Lee, A. S. L.; Li, Y.-S. Surface-enhanced Raman spectra using silver-coated paper substrates. *J. Raman Spectrosc.* **1994**, *25*, 209–214.

[20] Tseng, S. C.; Yu, C. C.; Wan, D. H.; Chen, H. L.; Wang, L. A.; Wu, M. C.; Su, W. F.; Han, H. C.; Chen, L. C. Eco-friendly plasmonic sensors: Using the photothermal effect to prepare metal nanoparticle-containing test papers for highly sensitive colorimetric detection. *Anal. Chem.* **2012**, *84*, 5140–5145.

[21] Wang, J. P.; Yang, L.; Liu, B. H.; Jiang, H. H.; Liu, R. Y.; Yang, J. W.; Han, G. M.; Mei, Q. S.; Zhang, Z. P. Inkjet-printed silver nanoparticle paper detects airborne species from crystalline explosives and their ultratrace residues in open environment. *Anal. Chem.* **2014**, *86*, 3338–3345.

[22] Yunker, P. J.; Still, T.; Lohr, M. A.; Yodh, A. G. Suppression of the coffee-ring effect by shape-dependent capillary interactions. *Nature* **2011**, *476*, 308–311.

[23] Lasch, P. Spectral pre-processing for biomedical vibrational spectroscopy and microspectroscopic imaging. *Chemom. Intell. Lab. Syst.* **2012**, *117*, 100–114.